Research Article

Chiara Schirripa Spagnolo*, Stefano Luin*

Setting up multicolour TIRF microscopy down to the single molecule level

https://doi.org/10.1515/bmc-2022-0032
received May 11, 2023; accepted June 26, 2023

Abstract: Investigating biological mechanisms in ever greater detail requires continuous advances in microscopy techniques and setups. Total internal reflection fluorescence (TIRF) microscopy is a well-established technique for visualizing processes on the cell membrane. TIRF allows studies down to the single molecule level, mainly in single-colour applications. Instead, multicolour setups are still limited. Here, we describe our strategies for implementing a multi-channel TIRF microscopy system capable of simultaneous two-channel excitation and detection, starting from a single-colour commercial setup. First, we report some applications at high molecule density and then focus on the challenges we faced for achieving the single molecule level simultaneously in different channels, showing that rigorous optimizations on the setup are needed to increase its sensitivity up to this point, from camera setting to background minimization. We also discuss our strategies regarding crucial points of fluorescent labelling for this type of experiment: labelling strategy, kind of probe, efficiency, and orthogonality of the reaction, all of which are aspects that can influence the achievable results. This work may provide useful guidelines for setting up advanced single-molecule multi-channel TIRF experiments to obtain insights into interaction mechanisms on the cell membrane of living cells.

Keywords: multi-channel TIRF microscopy, multicolour fluorescence microscopy, single-molecule imaging, cell membrane, neurotrophic receptors

*** Corresponding author: Chiara Schirripa Spagnolo,** NEST Laboratory, Scuola Normale Superiore, Piazza San Silvestro 12, I-56127, Pisa, Italy, e-mail: chiara.schirripaspagnolo@sns.it
*** Corresponding author: Stefano Luin,** NEST Laboratory, Scuola Normale Superiore, Piazza San Silvestro 12, I-56127, Pisa, Italy; NEST Laboratory, Istituto Nanoscienze-Consiglio Nazionale delle ricerche (CNR), Piazza San Silvestro 12, I-56127, Pisa, Italy, e-mail: s.luin@sns.it

Introduction

Total internal reflection fluorescence (TIRF) microscopy is the technique of choice to investigate a variety of biological processes that occur near to the cell membrane, such as endocytosis, exocytosis, cell adhesion, cytoskeletal dynamics, cell signalling, virus infection, and drug delivery [1–4]. It provides excitation on a thin layer (~100 nm) including the membrane adherent to the thin bottom-glass of the petri used in microscopy; the consequent elimination of background from deeper regions of the sample outstandingly improves the signal-to-noise ratio and the spatial resolution. Another benefit of this restricted excitation is the minimization of cell radiation exposure and associated toxicity.

Biological processes are determined and modulated by various cooperation and interaction mechanisms amongst cell structures and biomolecules, which form complex interaction networks.

In the context of cell membranes, for example, a synergy with the actin cytoskeleton has been observed for different kinds of receptors [5]. B-cell receptor signalling is influenced by actin dynamic organization, and actin dynamics is in turn modulated by receptor signalling [6]. Dynamic interactions with the actin cytoskeleton modulate the trafficking, ligand binding, and signalling capabilities of the neurotrophic receptor TrkA [7,8] as well as the AMPA receptor [9] or G protein-coupled receptors (GPCR) [10]. At the same time, membrane receptors show interactions with lipids that influence their functioning through mechanisms of conformational stabilization and the selection and consequent regulation of localization and partitioning, as has been observed for different types of receptors, such as GPCR, p75NTR, nicotinic acetylcholine, and epidermal growth factor [11–15]. Receptor signalling is also influenced by interactions with possible coreceptors, as in the case of neurotrophic signalling, which is modulated by cooperations between Trks and $p75^{NTR}$ [16–19] or of immune function in T cells, modulated by interactions between receptors of the CD28 and tumor necrosis factor receptor families [20]. Obviously, fundamental interactions that regulate receptor response are those with external ligands, signalling molecules, inhibitors, activators, drugs, and viruses.

Thus, several interaction mechanisms on the cell membrane regulate the functioning of receptors as well as other cellular processes. Multi-channel setups that allow the visualization of different entities are required to study these interactions by microscopy techniques. In particular, simultaneous (rather than sequential) multi-channel approaches are needed to study dynamics and relatively fast processes.

TIRF microscopy also allows for achieving the single-molecule level [21]. Single-channel single-molecule TIRF has become an exceptional approach for investigating the behaviour of one kind of molecule on the cell membrane since the single-molecule level has allowed exploring the heterogeneities of the membrane environment, revealing how they are related to molecular functions [22–24]. These heterogeneities affect molecular dynamics, as observable in single-channel studies, and interactions, which are detectable in multi-channel applications. Multi-channel single-molecule TIRF has been widely used for *in vitro* studies on molecules adherent to glass [25,26]. However, it is still a challenging technique especially on fast-moving molecules, because the signal-to-noise ratio is lowered by their movement during signal acquisition: achieving an adequate signal-to-noise ratio for the detection of weak single-molecule signals in multiple channels is still not a straightforward task, especially when using small organic dyes. This kind of probe allows minimizing alterations to molecular behaviour in comparison to larger nanoparticles like quantum dots, but at the price of a lower brightness and the need for multiple excitations for multi-channel studies [27,28]. Consequently, the limitations in the signal-to-noise ratio result from a combination of a limited number of specific photons emitted and a sum of background signals excited with different excitation wavelengths [29].

Here, we describe the methods we developed to achieve multicolour TIRF experiments down to the single-molecule level. First, we report an effective setting up of a two-colour microscopy starting from a TIRF commercial system that does not allow for simultaneous multicolour excitation and detection. Our strategy is cost-effective especially when TIRF microscopes are already in the laboratory and are not the latest commercial systems with multicolour capabilities. We then illustrate the optimizations required to achieve the single-molecule visualization level. In the next section, we discuss the careful selection of labelling strategy and fluorescent probes required for multicolour single-molecule experiments. Importantly, the observation of interactions (which is probably the main goal of a multicolour application) needs high and known labelling efficiencies and the possibility of orthogonal labelling on different molecules. Finally, we summarize some of the achieved applications of the illustrated methods.

Materials and methods

Cell cultures

SH-SY5Y (ECACC 94030304) and SK-N-BE(2) (ATCC® CRL-2271™) cell lines were maintained at 37°C, 5% CO_2 in DMEM/F-12 medium supplemented with 10% fetal bovine serum, 1% L-glutamine, 1% penicillin–streptomycin. 24 h before transfection, cells were seeded on glass-bottom dishes suitable for microscopy.

Receptor expression

We used human S6-tagged TrkA and $p75^{NTR}$ receptors, as previously described [8,14,30]. S6-TrkA was transfected in SH-SY5Y cells using Lipofectamine 2000 (Thermo Fisher Scientific) according to the manufacturers' instructions. S6-$p75^{NTR}$, inserted in a lentiviral transfer plasmid as previously described [14], was used both with and without reconstruction of lentiviral particles; in the latter case, the construct was simply transfected by Lipofectamine 2000. S6-$p75^{NTR}$ was expressed in SK-N-BE(2) cells: 5 h after the transfection, the expression was induced with doxycycline (with concentrations variable in the range 0.005–1 μg/ml depending on the desired expression density) added in the culture medium.

Synthesis of CoA-dyes

Synthesis of coenzyme A (CoA)-conjugated dyes was performed as previously described [7,29]. Briefly, coenzyme A was dissolved in tris(2-carboxyethyl)phosphine (TCEP) solution and then mixed with a solution of the maleimide-derivative of the dye dissolved in DMF. The reaction was stirred for 2–4 h at 37°C. The product was purified by high-performance liquid chromatography (Dionex Ultimate 3000; column: Phenomenex Kinetex EVO C-18 150 × 3.00 mm; solvents: ammonium acetate 10 mM, acetonitrile 95%). The product was lyophilized and stored at −20°C.

Fluorescent labelling

For two-colour experiments on $p75^{NTR}$ receptors and lipid rafts, SK-N-BE(2) cells were labelled as previously described [14]. Briefly, first, we labelled $p75^{NTR}$ receptors with CoA-Abberior STAR 635p, then we labelled and

crosslinked lipid rafts by using cholera toxin-subunit B (CT-B) conjugated with Alexa 488 and subsequently Anti-CT-B (Vybrant Alexa Fluor 488 Lipid Raft Labelling Kit, ThermoFisher Scientific). After each labelling step, cells were washed with PBS (cold in the case of raft staining, warm in the case of receptor staining). Receptor staining was performed at 37°C, and raft staining was performed at 4°C in cell medium.

For experiments in which either TrkA or $p75^{NTR}$ receptors were visualized simultaneously in two channels, receptors were labelled using a mixture of two dyes in the reaction (combinations of dyes are specified in the discussion of the experiments in the main text). Protocols for the labelling through Sfp PPTase were previously described [30,31].

Each sample was visualized under the microscope immediately after the labelling procedure.

TIRF microscopy

We used a Leica Microsystem AF6000 inverted epifluorescence wide-field microscope equipped with TIRF module, four laser lines (405, 488, 561, and 635 nm) switchable via an acousto-optic tuneable filter (AOTF), HCX PL APO 100.0× oil-immersion objective (NA = 1.47), EM-CCD camera (iXon Ultra 897, Andor), incubator chamber for maintaining 37°C, and 5% CO_2 conditions for live cell imaging (Leica AM TIRF MC). The microscope is provided with the Acquisition software LasAF (Leica Application Suite for Advanced Fluorescence).

For microscopy acquisitions, we usually select a region of interest (ROI) including the membrane of a labelled cell.

For two-colour imaging of $p75^{NTR}$ receptors and lipid rafts, we acquired 500-frame time series with an integration time of 21 ms, resulting in a frame time of 30 ms.

For two-colour single-molecule imaging and tracking of single receptors in both channels, we acquired 250-frame time series with an integration time of 40 ms, corresponding to a frame time of 56 ms.

Results and discussion

Multicolour TIRF microscopy setup

The simplest multicolour TIRF configurations are based on sequential imaging of different channels. This can be achieved by exploiting an AOTF, which replaced mechanical shutters in order to avoid moving components, control intensities, and obtain faster excitation switching (few microseconds) [32]. However, the feasibility of using these short switching times is limited by the readout time required by the camera and the exposure time needed to collect enough photons to obtain a sufficient signal-to-noise ratio, especially in advanced single-molecule studies. Indeed, typical image integration times are at least tens of milliseconds [7,14,33].

This time-shifting between the different channels makes it challenging to study interaction mechanisms, especially if they are dynamic, transient, and relatively fast, as for several kinds of complexes forming on the cell membrane [34,35].

Therefore, multiple simultaneous excitations and detection systems are required. Our laboratory was equipped with a typical commercial TIRF system (by Leica Microsystems, see Section 2) provided with four internal laser lines (405, 488, 561, 635 nm) that can be switched by an AOTF, but not be used simultaneously. We implemented a relatively simple but effective way to obtain real simultaneous excitation with two different laser lines in this setup. The output of the microscope laser box was connected to a 4-way fibre-coupled laser combiner (QiOptiq iFLEX-Adder™) via a polarization-maintaining fibre connected to the entry port for either 405, 561 or 635 nm, depending on the desired wavelength. A supplementary external laser (Qioptiq iFLEX-iRIS, 488 nm) was equipped with a single-mode fibre output, which was connected to the 488 nm input of the laser combiner. The output of the laser combiner was connected to the excitation entrance of the microscope through a polarization-maintaining fibre. KineMATIX® fibre couplers were used for aligning the single-mode fibres to the lasers at the external laser output and at the laser combiner inputs and outputs. This coupler system has four axes of alignment (X, Y, tip, tilt) with submicron repeatability and sub-microradian stability. The laser-fibre alignment is stable over temperature changes and for multiple fibre removal and insertion operations, with a positioning accuracy of 10 nm.

These setup modifications allowed for simultaneous double excitation using one of the original TIRF system's internal lasers and the additional 488 nm laser. The power of the internal lasers was controlled by the acquisition software provided by the microscope manufacturer (i.e. LASAF by Leica Microsystems). The power of the additional laser was controlled by applying the output of a digital-to-analog converter card fitted to a computer to its bayonet neill-concelman control connector. The acquisition software also allowed setting the TIRF penetration depth of the internal laser through the control of the incidence angle of the excitation beam. Since the system had a unique excitation path, the angle of incidence was the same also for the external 488 nm laser, resulting in a slight

difference in the penetration depth. For example, a penetration depth of 130 nm for the internal 635 nm laser line corresponded to a penetration depth of about 100 nm for the 488 nm line; a penetration depth of 115 nm for the internal 561 nm laser line corresponded to a penetration depth of about 100 nm for the 488 nm line. These differences allowed penetration depths of both wavelengths to be in the range of values typically used for TIRF imaging on cell membranes (without significantly exciting internal cellular structures in any channel) and did not compromise multi-channel quantitative studies [14,29].

To achieve simultaneous double detection of two different channels as well, we inserted a Dual-View™ system (Optical Insights DV-CC) in front of the camera. It is based on a dichroic filter that splits the incident light (i.e. the light leaving the microscope) into two independent beams: one reflected off, for wavelengths below the cut-off of the dichroic, and one transmitted, for wavelengths above the cut-off of the dichroic. This system can also perform beam splitting based on other properties different from wavelength, such as polarization through a polarizing beam splitter. Each produced beam is reflected by mirrors towards a spectral filter that defines its wavelength band (or towards other kinds of filters to select other properties). The two final beams pass through a common imaging lens that projects them on the same detector, each one over half of the detector area, forming two images of the same object with different information content, such as different spectral ranges.

The dichroic filter and the final two filters are included in a removable "Dual-View filter cube," so these filters can be customer specific. Different cubes can be easily interchanged depending on the user's needs. Inside each cube, the dichroic filter is fixed, and the filters can be removed or substituted.

We also added an Optomask adjustable field mask aperture (OPTMSK-L, Andor) between the microscope output and the DualView system. This component allows precise control of the aperture, thanks to four adjustable blades, and defines a sub-region of the detector for acquisition, masking pixels outside this area. Therefore, it can allow increasing the acquisition frame rate by limiting the illuminated area of the camera; this is especially useful for dynamic studies.

We implemented the whole two-colour TIRF system by using (i) simultaneous double excitation with the internal 635 nm laser plus the 488 nm external one; (ii) a fluorescence cube containing ZET488/640× excitation filter, ZT488/640rpc dichroic, ZET488/640 m emission filter (TRF59906 – ET – 488/640 nm Laser Dual Band Set for TIRF applications, Chroma); (iii) dichroic beam splitter T600lpxr and filters ET525-50 and r647lp (Chroma) in the DualView cube. This implementation allows the simultaneous observation of green-emitting dyes excitable at 488 nm (typical "488" dyes from several companies) and far-red-emitting dyes excitable at 635 nm (typical "635" or "640" dyes).

With this system, we visualized simultaneously in two channels $p75^{NTR}$ receptors expressed at high density and labelled with a mixture of Abberior STAR 635p and Abberior STAR 488 on the membrane of living cells (Figure 1).

Reaching the single-molecule level: optimization of camera parameters

TIRF microscopy is an optimal technique for obtaining single-molecule level visualization on the cell membrane [21]. However, we observed that single-molecule imaging requires careful settings of camera parameters to obtain the best compromise between time resolution and signal-to-noise ratio, especially for dynamic studies. We performed our optimizations of camera parameters at a fixed frame time of 30 ms, which is a typical value used for dynamic single-molecule imaging (and tracking) [34,37].

The following parameters related to a signal readout of the EMCCD (electron multiplying charge-coupled devices) camera could be tuned with the acquisition software: horizontal shift speed of charges in the read registry (pixel clocking rate); vertical shift speed of charges from one row on the EMCCD sensor to the next (vertical shift speed); voltage amplitude for charge rows shifting (vertical clock voltage) (Figure 2). Temperature can also be tuned: it was set to −75°C to reduce dark current.

The pixel clocking rate was set to 17,000 MHz, the maximum value for our camera, in order to maximize the rate at which pixels are read from the shift register and, therefore, the frame rate.

The vertical shift speed of our camera could be varied between 0.5 and 3.3 µs. The vertical clock voltage had the following possible settings: "Normal," +1, +2, +3, +4. The first one is the default value (set at the factory in camera testing); the others indicate the voltage increase compared to the "Normal."

The maximum vertical shift speed (corresponding to the minimum time value setting of 0.5 µs) allows the shortest frame time, which is our goal in order to achieve the best temporal resolutions. It also allows minimizing the clock induced charge (CIC, i.e. spurious electrons created during charge shift), as we verified by measuring the mean and standard deviation of the intensities of pixels in non-illuminated EMCCD areas (Figure 2b): both are lower with a vertical shift speed of 0.5 µs than with 3.3 µs, especially at

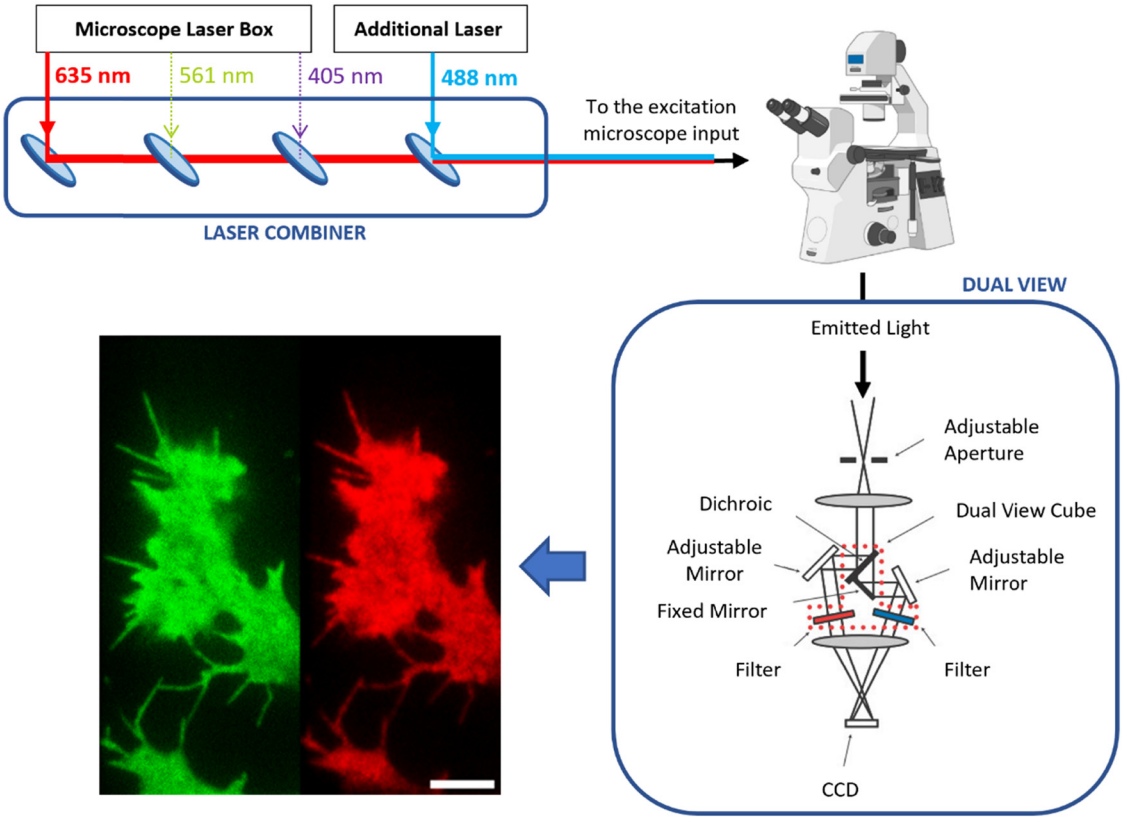

Figure 1: Multicolour TIRF microscopy setup. Top left: simultaneous double excitation is obtained by using the 635 nm laser of the microscope laser box and an additional 488 nm laser. Both enter a laser combiner and the final combined beam reaches the excitation input of the microscope. Bottom right: simultaneous double detection is achieved through the DualView system in which the emitted light is split into two beams by a dichroic and filters; each beam is projected onto one half of the same CCD (charge-coupled device) camera. The scheme of the DualView is reprinted with permission of Teledyne Photometrics, Tucson, Arizona [36]. Bottom left: example of an image obtained with the schematized setup. $p75^{NTR}$ receptors expressed on the membrane of living human neuroblastoma cells were labelled with a mixture of Abberior Star635p and Abberior Star488 and visualized simultaneously in two channels; a green and a red intensity scale was applied to the left and right part of the image; scale bar: 5 µm.

a higher vertical clock voltages (Figure 2b). However, the charge transfer efficiency is reduced with faster vertical speeds, and a pixel could leave a significant charge behind. Indeed, we observed that by setting the vertical shift speed to 0.5 µs and the vertical clock voltage to "Normal," there was a smearing effect on the spots of single dye molecules (Figure 2c). This effect can be eliminated by increasing the voltage amplitude, which, however, must be limited to limit the creation of spurious CICs. Indeed, we observed that as the vertical clock voltage increases, the mean and standard deviation of the intensity in non-illuminated EMCCD areas also increase (Figure 2d). We found out that the minimum vertical clock voltage that allowed avoiding spot smearing at the vertical shift speed of 0.5 µs, was "+2" (compare Figure 2c with the images of single molecules shown in the following figures).

Reaching the single-molecule level: background reduction

Due to excitation limited to a restricted region close to the coverglass–water interface, TIRF microscopy minimizes background from the out-of-focus inner regions of the cell, significantly improving the signal-to-noise ratio. The background reduction inherent to the TIRF principle has largely proven powerful for single-channel single-colour measurements. However, some background sources are still excited in TIRF, such as optical components in the light path or sample elements other than the ones of interest. Reaching multicolour single-molecule TIRF requires careful investigation and control of these background and noise sources, especially when using small, minimally invasive organic dyes for fluorescent labelling (see also Section 3.4) [27,29].

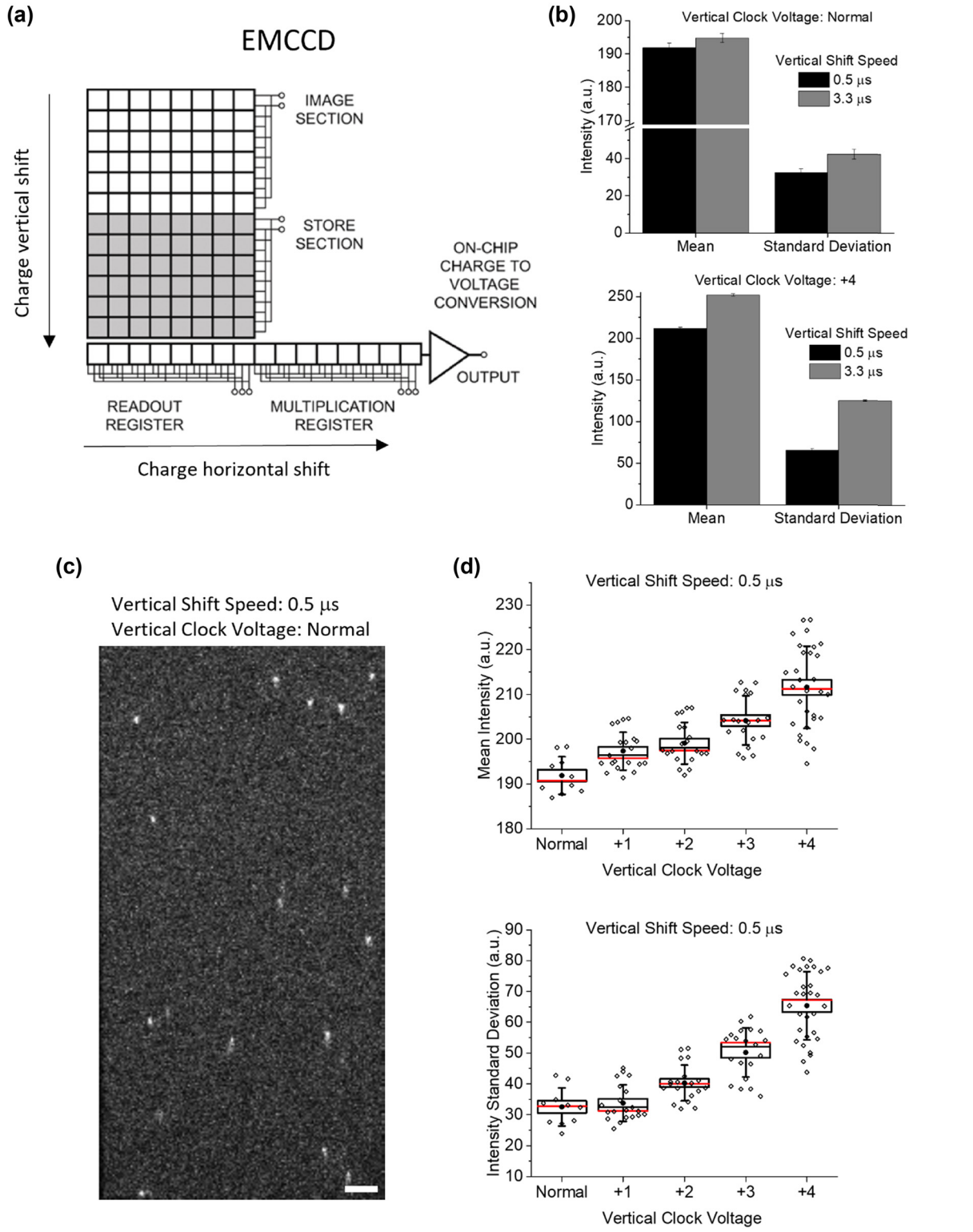

Figure 2: Single-molecule imaging requires optimization of camera parameters. (a) Redout scheme of an EMCCD. The charges accumulated in the image section are shifted in the store section and towards the readout register (vertical shift), where are led to the multiplication register (horizontal shift) and finally to the voltage converter. Image reprinted with permission from [38] (Copyright © 2020 Oxford Instruments plc, Tubney Woods, Abingdon, Oxon OX13 5QX, UK All Rights Reserved). (b) Mean and standard deviation of the pixel intensities detected in non-illuminated EMCCD areas with different redout parameters (vertical shift speed and clock voltage, as stated on the graphs). Data are mean ± SEM obtained from 10 to 30 measurements from two independent repetitions. (c) Effect of spot smearing observed on single dye molecules when a high vertical speed is used but voltage amplitude is not sufficient for efficient charge shifting. (d) Mean (top) and standard deviation (bottom) of the pixel intensities detected in non-illuminated EMCCD areas using a vertical shift speed of 0.5 µs and different clock voltages. Box: SEM; whisker: SD; red line: median; filled circle: mean; empty diamonds: individual measurements, from two independent repetitions.

Our first setup implementation was based on a first channel excited at 488 nm detected in the green region and a second channel excited at 635 nm detected in the far-red region. We were able to visualise receptors expressed and labelled at high densities (in comparison to single-molecule level) in both channels (Figure 1) or to visualise a receptor at the single-molecule level in one channel (the 635 channel) and crosslinked membrane molecules in the other (the 488 one, Figure 3) [14]. However, we observed a significant level of background detected in the far-red channel when switching on the excitation at 488 nm. This behaviour hampered experiments at the single molecule level in both channels (Figure 4). Indeed, when the 488 channel was employed for the observation of cross-linked molecules, the laser power could be kept low (typically 0.178 mW at the objective [14]); but we needed higher powers, typically around 3 mW, for detecting single molecules labelled with organic dyes. Such excitation powers at 488 nm caused a background in the far-red channel that was too high to detect single molecules of the 635 dye (Figure 4). Measuring the transmission spectra of the used filters with a spectrophotometer (Jasco V-550) ruled out that the phenomenon was due to poor performance of theirs. Thus, we assumed

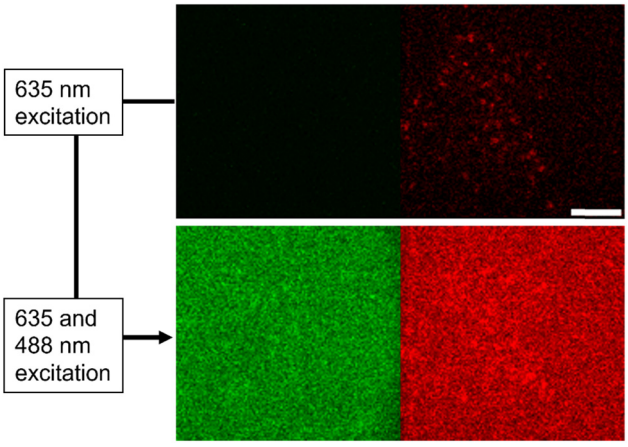

Figure 4: Background hindering single-molecule detection. Each of the two images is acquired with the two-colour TIRF setup and has on the left the channel corresponding to 488 nm excitation and green detection (500–550 nm) and on the right the channel corresponding to 635 nm excitation and far-red detection (650–750 nm), as described in the main text. Top: single molecules of Abberior STAR 635p labelling TrkA receptors were visualized under single excitation at 635 nm. Bottom: the same field of view was imaged by also turning on the excitation at 488 nm which resulted in a background masking individual molecules in the far red. A green and a red intensity scale was applied to the left and right part of the image; scale bar: 5 µm.

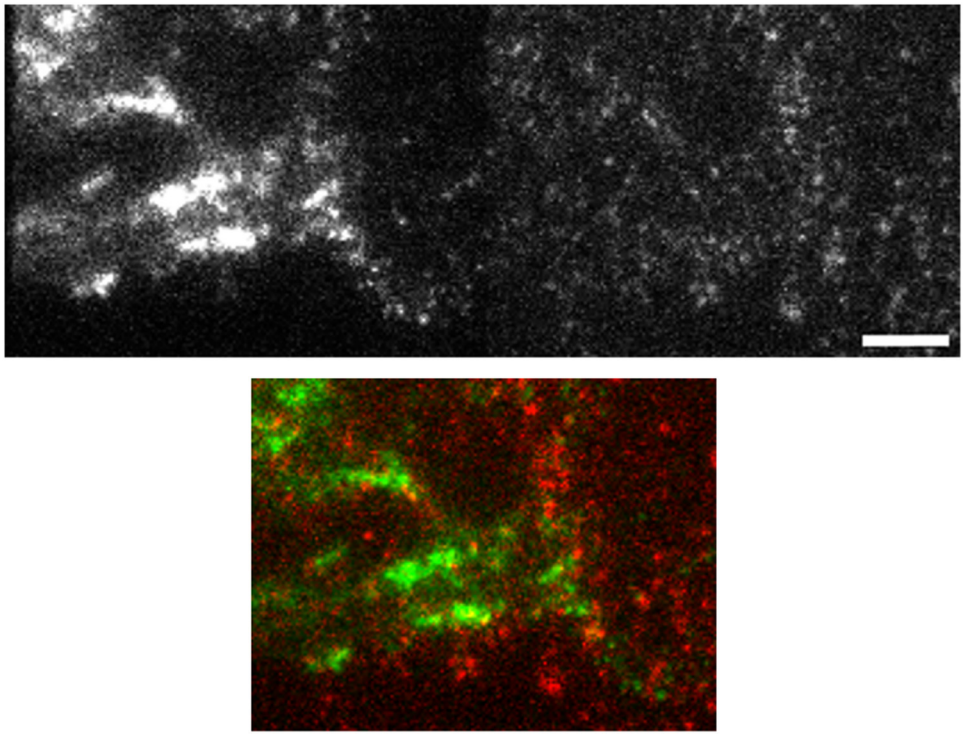

Figure 3: Two-colour TIRF experiment on $p75^{NTR}$ receptors and lipid rafts. $p75^{NTR}$ receptors were labelled with Abberior STAR 635p, lipid rafts were labelled with Alexa 488. The two dyes were simultaneously visualized in TIRF. Top: example of an acquired image (lipid raft, left channel; single molecule of $p75^{NTR}$ receptor: right channel). Bottom: overlap of the two channels; lipid rafts: green, $p75^{NTR}$ receptor: red. Scale bar: 5 µm.

that the background signal was actually originating from some elements inside the setup that under 488 nm excitation emit in the far-red region. Indeed, this type of behaviour was compatible with possible autofluorescence phenomena originating from optical glasses.

The fluorescence of glasses can be generated by various factors, such as colour centres (e.g. rare earth elements or other ions) or by the structural units of the glass matrix, also depending on its processing [39,40]. In particular, the red emission is often associated with non-bridging oxygen hole centres [41,42]. Several elements of the microscopy system can contribute to this emission from the optical glass, such as coverslip, objective lens assembly, other lenses and filters [43,44]. We found a significant reduction of the background detected in the longer-wavelength channel ("second channel") under excitation at the shorter wavelength by shifting the detection band of the second channel from the red to the orange region [29]. So, we modified the configuration of the setup as follows: we used the internal 561 nm laser line instead of the 635 nm one and continued to use the external 488 nm laser as additional excitation. We replaced the fluorescence cube with a Quad 405/488/561/640 nm; we replaced the DualView cube, using one with Chroma 565dcxr dichroic beam splitter and Chroma ET525-50 and Semrock FF01-600/52 filters. This setup allowed for the simultaneous observation of green-emitting dyes excitable at 488 nm (typical "488" dyes from different companies) and orange-emitting dyes excitable at 561 nm (typical "561" or "565" dyes). This new implementation enabled an improved signal-to-noise ratio in the channel at longer wavelengths and the simultaneous visualization of single molecules in both channels. We tested the system on the observation of TrkA receptors simultaneously labelled with a mix of Atto 488 and Atto 565 dyes on the membrane of living cells (Figure 5).

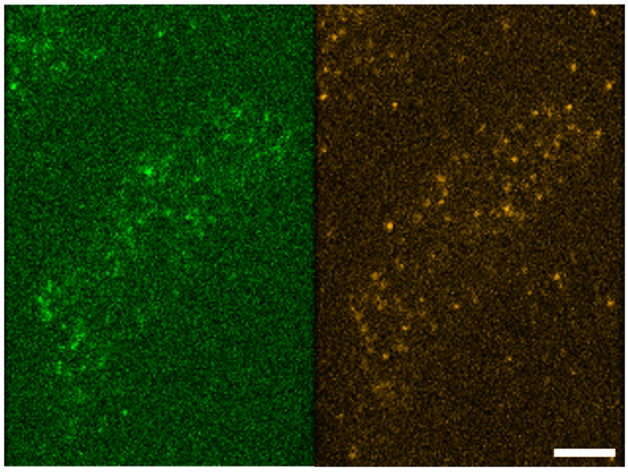

Figure 5: Two-colour TIRF single-molecule imaging. TrkA receptors expressed on the membrane of living cells were labelled with a mixture of Atto 488 (left part of the image) and Atto 565 (right part of the image); the two channels are acquired in TIRF under simultaneous double excitation and detection. A green and an orange intensity scale was applied to the left and right part of the image; scale bar: 5 μm.

Fluorescent labelling: choice of the probe, efficiency and orthogonality

Nowadays, fluorescent labelling of biomolecules can be performed by several conjugation strategies and with several probes [27,45–48]. Single-molecule applications require very careful selection of the optimal approach, which must ensure adequate signal-to-noise ratio, specific and efficient molecule-probe conjugation, controlled molecule-probe stoichiometry, no perturbation on the observed process, high photostability, and low non-specific interactions [27,49,50]. Multi-channel studies further require the minimization of crosstalk and bleedthrough between different dyes and, especially in the case of multiple excitation sources, also require the limitation of (possibly "cross"-excited) background and noise emissions, which can easily hide dim signals from single molecules [27,29]. We chose to exploit labelling based on short ACP-derived peptide tags (e.g. S6, A1 composed of 12 amino acids) that can be genetically inserted into molecular sequences and conjugated to the probe via an enzymatic reaction (based on phosphopantetheinyl transferases, PPTase) [30,51]. This strategy is site-specific on the molecule of interest, thus allowing control of the conjugation site; this is useful for not altering molecular functions such as interactions of a labelled receptor with its ligands or of a labelled ligand with its receptors [52]. It has been demonstrated that this kind of labelling does not alter the functions of neurotrophin ligands and receptors [30]. Moreover, this labelling approach results in a controlled 1:1 molecule:probe stoichiometry, which is a property needed, especially for the investigation of molecular complexes and the estimation of their stoichiometries (i.e. dimeric, trimeric, or higher orders) [7,53]. The involved tags are versatile and can be conjugated with different classes of probes carried by CoA substrates. Indeed, this kind of labelling has been performed with quantum dots (Qdots) as well as organic dyes [7,8,14,53].

Setting up our approach for multicolour single-molecule experiments, we considered that small organic dyes (typical size ~1 nm) allow minimizing alterations and steric hindrance in comparison to more cumbersome Qdots (typical size tens of nanometres), as also observed in the

literature [14,28]. Moreover, the goal of multicolour studies is the visualization of interactions; this requires high and known labelling efficiencies (e.g. a dimeric interaction can only be detected if both the molecules involved are labelled). These can be achieved by labelling with organic dyes, while it is still challenging in the case of Qdots [27]. After choosing the labelling strategy and the kind of fluorescent probe, we developed a method to control and measure the labelling efficiency in the experimental condition of interest [54]. This is a crucial point, despite the availability of labelling protocols, in fact some conditions that ensure high labelling efficiency are actually not applicable in single-molecule experiments due to the high density of spots spuriously adhered to the cells and coverslip [27,49,54]. Our method is based on the fact that a labelling reaction with 100% efficiency leaves no molecule unlabelled among the accessible ones; instead, a labelling reaction with lower efficiency leaves a certain percentage of unlabelled molecules dependent on the efficiency value (Figure 6). Unlabelled molecules can be visualized by performing a subsequent labelling reaction on the same sample with a second different probe: a certain percentage will be detected depending on the efficiency of the second reaction (Figure 6). In addition to qualitatively visualizing whether the first reaction had left unlabelled molecules, the method allows for quantitative measurements: the ratio between the number of molecules labelled with the two different probes can be measured and used for calculating the desired labelling efficiency with high accuracy. For further details, we refer to the study of Schirripa Spagnolo et al. [54].

For studying interactions between different kinds of molecules, another requirement in labelling, in addition to efficiency, is orthogonality. The use of ACP-derived tags allows orthogonal labelling by exploiting two different tags (A1 and S6) selectively labelled by two different PPTases, Sfp and AcpS [30,55]. This has been demonstrated *in vitro* and in living cells; in the latter case, we recall the orthogonal labelling of S6-EGFR (epidermal growth factor receptor) and A1-TfR1 (transferrin receptor 1) [55] and of S6-TrkA and A1-P75NTR [30].

Of note, performing single-molecule experiments at high labelling efficiency requires molecular expression at the single-molecule level. In some cases, common lipid-mediated transfections can lead to this desired density, possibly optimizing transfection conditions and time [33]; in other cases, other transfection methods must be applied that allow the control of gene expression. This strongly depends on the experimental conditions, especially cell line and molecule to be expressed. In our case, we observed that the TrkA receptor can reach single-molecule expression with standard lipid-based transfection, contrary to the p75; for the latter, we exploited inducible lentiviral expression vectors [31,56].

Summary of applications

As we mentioned in previous sections, the first application of the implemented two-colour TIRF setup was aimed at the simultaneous visualization of the $p75^{NTR}$ receptor and

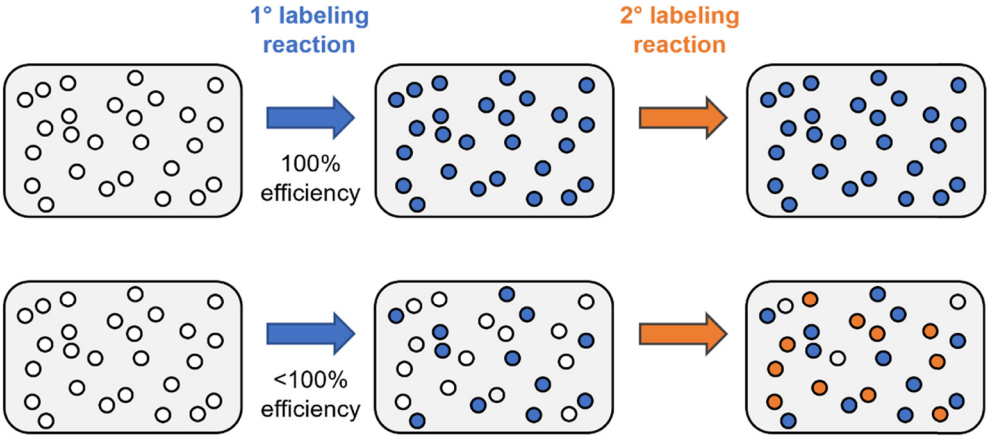

Figure 6: Principle for detecting the efficiency of a fluorescent labelling reaction. The small circles in the boxes represent the molecules, white: unlabelled, blue or orange: labelled. Top: The fluorescent labelling reaction of interest (in blue) has an efficiency of 100%: it does not leave unlabelled molecules. If the same sample is subjected to a second labelling reaction with a different probe (orange), the latter does not label any molecules. Bottom: The fluorescent labelling reaction of interest (in blue) has an efficiency of less than 100%: it leaves some unlabelled molecules. If the same sample is subjected to a second labelling reaction with a different probe (orange), the latter labels some molecules.

of cross-linked lipid rafts (see Material and Methods) on the membrane of living cells [14]. These membrane regions are crucial areas for the signalling activity of different types of receptors [57–59]. The two-colour experiment allowed studying the partition of the receptor inside and outside these membrane areas after binding with nerve growth factor (NGF). Both the wild-type receptor and a mutated form, lacking some residues considered crucial for dimerization in the previous literature, were studied. It has been observed that the wild-type receptor increases its mean residency in the lipid rafts regions under NGF stimulation, contrary to the mutated form. This observation was paramount for devising a model of receptor activation in which its localization in specific membrane regions, and not its dimerization, is the key mechanism for its activity; moreover, some essential domains for these partitioning mechanisms were identified [14].

We also performed some proof-of-concept applications for simultaneous two-colour imaging of neurotrophin receptors on the cell membrane, down to the single-molecule level in both channels. We applied the two-colour TIRF setup to visualize either TrkA or $p75^{NTR}$ receptors, each one simultaneously in two channels. In each experiment, the fluorescent labelling was performed on cells expressing one of the two receptors using a mixture of two spectrally distinct dyes in the reaction, so that some receptors were labelled with a dye and some with the other one [29,54]. The receptors were imaged at different densities, from high ones down to the single-molecule level (Figures 1 and 5), and in the last case, we were able to perform simultaneous two-colour single-molecule tracking [29]. Furthermore, by using a method we developed for measuring labelling efficiency, we could thoroughly optimize labelling reaction conditions and demonstrated single-molecule imaging at high labelling efficiency and low aspecific background (Figure 5, [29,54]).

Conclusions and perspectives

In this work, we presented or reviewed the strategies we implemented for setting up a TIRF microscope to perform simultaneous two-channel imaging with simultaneous double excitation and detection, down to the single-molecule level. First, we discussed the components incorporated into a commercial single-colour system to expand its potential towards multicolour imaging. After performing some initial experiments at higher molecule densities, we showed that increasing sensitivity towards the single-molecule level and towards even more accurate analysis requires even deeper optimizations of the system. We report the importance of optimizing camera parameters and finding the background and noise sources in the system. We also addressed some issues related to the fluorescent labelling of the sample: we explained our choice of fluorescent labelling strategy and type of fluorescent probe; both are primarily motivated by the requirement of minimising alteration in molecular behaviour. We highlighted the importance of controlling and knowing the yield of the used labelling reaction and of achieving orthogonal labelling of different molecules, with an explanation of the approaches we adopted.

The methods described here can be applied to investigate interaction mechanisms on the membrane of living cells. In particular, interactions between a molecule and specific membrane structures can be studied analogously to the shown example on p75 receptor and lipid rafts; moreover, the visualization of a single kind of molecule labelled with a mixture of two different dyes can be exploited to study homodimerization processes; while by using orthogonal labelling of two different molecules, hetero-interaction mechanisms can be investigated.

Acknowledgments: We thank Laura Marchetti and Fulvio Bonsignore for preparation of constructs and help in cell culture and Aldo Moscardini for help in synthesis of CoA-dyes.

Funding information: This research received funding from Scuola Normale Superiore (SNS16C_B_LUIN, SNS_RB_LUIN, SNS19_A_LUIN) and from Fondazione Pisa (project Nanotechnology for tumour molecular fingerprinting and early diagnosis, RST 148/16).

Conflict of interest: Authors state no conflict of interest.

Data availability statement: The datasets generated during and/or analysed during the current study are available from the corresponding authors on reasonable request.

References

[1] Rao TC, Nawara TJ, Mattheyses AL. Live-cell total internal reflection fluorescence (TIRF) microscopy to investigate protein internalization dynamics. In Methods in Molecular Biology. New York, NY, USA: Humana Press Inc; 2022. p. 45–58.

[2] Müller M, Lauster D, Wildenauer HHK, Herrmann A, Block S. Mobility-based quantification of multivalent virus-receptor interactions: New insights into influenza A virus binding mode. Nano Lett. 2019;19(3):1875–82.

[3] Jing H, Pálmai M, Saed B, George A, Snee PT, Hu YS. Cytosolic delivery of membrane-penetrating QDs into T cell lymphocytes:

Implications in immunotherapy and drug delivery. Nanoscale. 2021;13(10):5519–29.
[4] Poulter NS, Pitkeathly WTE, Smith PJ, Rappoport JZ. The physical basis of total internal reflection fluorescence (Tirf) microscopy and its cellular applications. Methods Mol Biol. 2014;1251:1–23.
[5] Mattila PK, Batista FD, Treanor B. Dynamics of the actin cytoskeleton mediates receptor cross talk: An emerging concept in tuning receptor signaling. J Cell Biol. 2016;212(3):267–80.
[6] Li J, Yin W, Jing Y, Kang D, Yang L, Cheng J, et al. The coordination between B cell receptor signaling and the actin cytoskeleton during B cell activation. Front Immunol. 2019;9(JAN):3096.
[7] Marchetti L, Callegari A, Luin S, Signore G, Viegi A, Beltram F, et al. Ligand signature in the membrane dynamics of single TrkA receptor molecules. J Cell Sci. 2013;126(19):4445–56.
[8] Amodeo R, Nifosì R, Giacomelli C, Ravelli C, La Rosa L, Callegari A, et al. Molecular insight on the altered membrane trafficking of TrkA kinase dead mutants. Biochim Biophys Acta - Mol Cell Res. 2020;1867(2):118614.
[9] Hanley JG. Actin-dependent mechanisms in AMPA receptor trafficking. Front Cell Neurosci. 2014;8(November):113585.
[10] Shrivastava S, Sarkar P, Preira P, Salomé L, Chattopadhyay A. Role of actin cytoskeleton in dynamics and function of the serotonin1A receptor. Biophys J. 2020;118(4):944–56.
[11] Baenziger JE, Hénault CM, Therien JPD, Sun J. Nicotinic acetylcholine receptor–lipid interactions: Mechanistic insight and biological function. Biochim Biophys Acta - Biomembr. 2015;1848(9):1806–17.
[12] Sarkar P, Mozumder S, Bej A, Mukherjee S, Sengupta J, Chattopadhyay A. Structure, dynamics and lipid interactions of serotonin receptors: excitements and challenges. Biophys Rev. 2021;13(1):101–22.
[13] Song W, Yen HY, Robinson CV, Sansom MSP. State-dependent lipid Interactions with the A2a receptor revealed by MD simulations using in vivo-mimetic membranes. Structure. 2019;27(2):392–403.e3.
[14] Marchetti L, Bonsignore F, Gobbo F, Amodeo R, Calvello M, Jacob A, et al. Fast-diffusing p75 ^{NTR} monomers support apoptosis and growth cone collapse by neurotrophin ligands. Proc Natl Acad Sci. 2019;116(43):21563–72.
[15] Hedger G, Shorthouse D, Koldsø H, Sansom MSP. Free energy landscape of lipid interactions with regulatory binding sites on the transmembrane domain of the EGF receptor. J Phys Chem B. 2016;120(33):8154–63.
[16] Conroy JN, Coulson EJ. High-affinity TrkA and p75 neurotrophin receptor complexes: A twisted affair. J Biol Chem. 2022;298(3):101568.
[17] Dechant G. Molecular interactions between neurotrophin receptors. Cell Tissue Res. 2001;305(2):229–38.
[18] Franco ML, Nadezhdin KD, Light TP, Goncharuk SA, Soler-Lopez A, Ahmed F, et al. Interaction between the transmembrane domains of neurotrophin receptors p75 and TrkA mediates their reciprocal activation. J Biol Chem. 2021;297(2):100926.
[19] Marchetti L, Luin S, Bonsignore F, de Nadai T, Beltram F, Cattaneo A. Ligand-induced dynamics of neurotrophin receptors investigated by single-molecule imaging approaches. Int J Mol Sci. 2015;16(1):1949–79.
[20] Gonzalez LC, Loyet KM, Calemine-Fenaux J, Chauhan V, Wranik B, Ouyang W, et al. A coreceptor interaction between the CD28 and TNF receptor family members B and T lymphocyte attenuator and herpesvirus entry mediator. Proc Natl Acad Sci U S A. 2005;102(4):1116–21.
[21] Shashkova S, Leake MC. Single-molecule fluorescence microscopy review: shedding new light on old problems. Biosci Rep. 2017;37(4):BSR20170031.
[22] Mashanov GI, Nenasheva TA, Mashanova A, Lape R, Birdsall NJM, Sivilotti L, et al. Heterogeneity of cell membrane structure studied by single molecule tracking. Faraday Discuss. 2021;232:358–74.
[23] Mohammad I-L, Mateos B, Pons M. The disordered boundary of the cell: emerging properties of membrane-bound intrinsically disordered proteins. Biomol Concepts. 2019;10(1):25–36.
[24] Redpath GMI, Betzler VM, Rossatti P, Rossy J. Membrane heterogeneity controls cellular endocytic trafficking. Front Cell Dev Biol. 2020;8:757.
[25] Churchman LS, Ökten Z, Rock RS, Dawson JF, Spudich JA. Single molecule high-resolution colocalization of Cy3 and Cy5 attached to macromolecules measures intramolecular distances through time. Proc Natl Acad Sci U S A. 2005;102(5):1419–23.
[26] Roy R, Hohng S, Ha T. A practical guide to single-molecule FRET. Nat Methods. 2008;5:507–16.
[27] Schirripa Spagnolo C, Luin S. Choosing the probe for single-molecule fluorescence microscopy. Int J Mol Sci. 2022;23(23):14949.
[28] Abraham L, Lu HY, Falcão RC, Scurll J, Jou T, Irwin B, et al. Limitations of Qdot labelling compared to directly-conjugated probes for single particle tracking of B cell receptor mobility. Sci Rep. 2017;7(1):1–13.
[29] Schirripa Spagnolo C, Moscardini A, Amodeo R, Beltram F, Luin S. Optimized two-color single-molecule tracking of fast-diffusing membrane receptors. bioRxiv. 2023;2023.03.17.533099.
[30] Marchetti L, De Nadai T, Bonsignore F, Calvello M, Signore G, Viegi A, et al. Site-specific labeling of neurotrophins and their receptors via short and versatile peptide tags. PLoS One. 2014;9(11):e113708.
[31] Gobbo F, Bonsignore F, Amodeo R, Cattaneo A, Marchetti L. Site-specific direct labeling of neurotrophins and their receptors: From biochemistry to advanced imaging applications. In Methods in Molecular Biology. New York, NY, USA: Humana Press Inc; 2018. p. 295–314.
[32] Sobhy MA, Elshenawy MM, Takahashi M, Whitman BH, Walter NG, Hamdan SM. Versatile single-molecule multi-color excitation and detection fluorescence setup for studying biomolecular dynamics. Rev Sci Instrum. 2011;82(11):113702.
[33] Calebiro D, Rieken F, Wagner J, Sungkaworn T, Zabel U, Borzi A, et al. Single-molecule analysis of fluorescently labeled G-protein-coupled receptors reveals complexes with distinct dynamics and organization. Proc Natl Acad Sci. 2013;110(2):743–8.
[34] Kasai RS, Suzuki KGN, Prossnitz ER, Koyama-Honda I, Nakada C, Fujiwara TK, et al. Full characterization of GPCR monomer–dimer dynamic equilibrium by single molecule imaging. J Cell Biol. 2011;192(3):463–80.
[35] Calebiro D, Sungkaworn T. Single-molecule imaging of GPCR interactions. Trends Pharmacol Sci. 2018;39(2):109–22.
[36] Advanced Imaging Camera Technology | Teledyne Photometrics [Internet]. [cited 2023 May 11]. https://www.photometrics.com/.
[37] Tsunoyama TA, Watanabe Y, Goto J, Naito K, Kasai RS, Suzuki KGN, et al. Super-long single-molecule tracking reveals dynamic-anchorage-induced integrin function. Nat Chem Biol. 2018;14(5):497–506.
[38] What is an EMCCD Camera? - Oxford Instruments [Internet]. [cited 2023 May 10]. https://andor.oxinst.com/learning/view/article/electron-multiplying-ccd-cameras.

[39] Jedamzik R, Pleitz J, Engel A, Petzold U, Elsmann F. Introducing the quantum efficiency of fluorescence of SCHOTT optical glasses. In: Johnson RB, Mahajan VN, Thibault S, editors. Current developments in lens design and optical engineering XVIII. San Diego, California, United States: SPIE Optical Engineering + Applications; 2017. p. 7.
[40] Kreidl NJ. Recent studies on the fluorescence of glass. J Opt Soc Am. 1945;35(4):249.
[41] Maes CF, Yan C. Laser-induced fluorescence in fused silica and other optical materials. In: Menzel ER, Katzir A, editors. Fluorescence detection IV. San Jose, CA, United States: SPIE; 1996. p. 93–102.
[42] Chan JW, Huser TR, Risbud SH, Krol DM. Modification of the fused silica glass network associated with waveguide fabrication using femtosecond laser pulses. Appl Phys A Mater Sci Process. 2003;76(3):367–72.
[43] Morgan CG, Mitchell AC. Total internal reflection fluorescence imaging using an upconverting cover slip for multicolour evanescent excitation. J Microsc. 2006;222(1):48–57.
[44] Grace J, Edlou S, Foss J, Hodgson C, Rheault JP, Rosvold J, et al. Using optical interference filters to measure autofluorescence in substrates and coatings. Surf Coat Technol. 2021;426:127777.
[45] Sahoo H. Fluorescent labeling techniques in biomolecules: A flashback. RSC Adv. 2012;2(18):7017.
[46] Freidel C, Kaloyanova S, Peneva K. Chemical tags for site-specific fluorescent labeling of biomolecules. Amino Acids. 2016;48(6):1357–72.
[47] Birke R, Ast J, Roosen DA, Lee J, Roßmann K, Huhn C, et al. Sulfonated red and far-red rhodamines to visualize SNAP- and Halo-tagged cell surface proteins. Org Biomol Chem. 2022;20(30):5967–80.
[48] Resch-Genger U, Grabolle M, Cavaliere-Jaricot S, Nitschke R, Nann T. Quantum dots versus organic dyes as fluorescent labels. Nat Methods. 2008;5(9):763–75.
[49] Zhang Z, Yomo D, Gradinaru C. Choosing the right fluorophore for single-molecule fluorescence studies in a lipid environment. Biochim Biophys Acta - Biomembr. 2017;1859(7):1242–53.
[50] Amodeo R, Convertino D, Calvello M, Ceccarelli L, Bonsignore F, Ravelli C, et al. Fluorolabeling of the PPTase-related chemical tags: Comparative study of different membrane receptors and different fluorophores in the labeling reactions. Front Mol Biosci. 2020;7:195.
[51] Yin J, Straight PD, McLoughlin SM, Zhou Z, Lin AJ, Golan DE, et al. Genetically encoded short peptide tag for versatile protein labeling by Sfp phosphopantetheinyl transferase. Proc Natl Acad Sci. 2005;102(44):15815–20.
[52] Di Matteo P, Calvello M, Luin S, Marchetti L, Cattaneo A. An optimized procedure for the site-directed labeling of NGF and proNGF for imaging purposes. Front Mol Biosci. 2017;4(FEB):4.
[53] Marchetti L, Bonsignore F, Amodeo R, Schirripa Spagnolo C, Moscardini A, Gobbo F, et al. Single molecule tracking and spectroscopy unveils molecular details in function and interactions of membrane receptors. In: Gregor I, Erdmann R, Koberling F, editors. Single molecule spectroscopy and superresolution imaging XIV. SPIE; 2021. p. 20.
[54] Schirripa Spagnolo C, Moscardini A, Amodeo R, Beltram F, Luin S. Quantitative determination of fluorescence labeling implemented in cell cultures. bioRxiv. 2023;2023.03.27.534369.
[55] Zhou Z, Cironi P, Lin AJ, Xu Y, Hrvatin S, Golan DE, et al. Genetically encoded short peptide tags for orthogonal protein labeling by Sfp and AcpS phosphopantetheinyl transferases. ACS Chem Biol. 2007;2(5):337–46.
[56] Barde I, Zanta-Boussif MA, Paisant S, Leboeuf M, Rameau P, Delenda C, et al. Efficient control of gene expression in the hematopoietic system using a single Tet-on inducible lentiviral vector. Mol Ther. 2006;13(2):382–90.
[57] Mollinedo F, Gajate C. Lipid rafts as signaling hubs in cancer cell survival/death and invasion: Implications in tumor progression and therapy. J Lipid Res. 2020;61(5):611–35.
[58] Zabroski IO, Nugent MA. Lipid raft association stabilizes VEGF receptor 2 in endothelial cells. Int J Mol Sci. 2021;22(2):1–15.
[59] Bisel B, Pavone FS, Calamai M. GM1 and GM2 gangliosides: recent developments. Biomol Concepts. 2014;5(1):87–93.